Tellus (2007), 59B, 303–317
Printed in Singapore. All rights reserved

TELLUS

Anthropogenic $\delta^{13}C$ changes in the North Pacific Ocean reconstructed using a multiparameter mixing approach (MIX)

By ROLF E. SONNERUP[1*], ANN P. McNICHOL[2], PAUL D. QUAY[3], RICHARD H. GAMMON[3], JOHN L. BULLISTER[4], CHRISTOPHER L. SABINE[4] and RICHARD D. SLATER[5], [1]*Joint Institute for Study of the Atmosphere and Ocean, University of Washington, Box 357941, Seattle, Washington, 98195, USA;* [2]*National Ocean Sciences AMS Facility, Woods Hole Oceanographic Institution, Woods Hole, Massachusetts, USA;* [3]*School of Oceanography, University of Washington, Seattle, Washington, USA;* [4]*NOAA/Pacific Marine Environmental Laboratory, Seattle, Washington, USA;* [5]*AOS program, Princeton University, Princeton, New Jersey, USA*

(Manuscript received 3 May 2006; in final form 9 January 2007)

ABSTRACT

A multiparameter mixing approach, 'MIX', for determining oceanic anthropogenic CO_2 was used to reconstruct the industrial-era change in the $^{13}C/^{12}C$ of dissolved inorganic carbon ($\delta^{13}C$ of DIC) along the 1992 165°E WOCE P13N section in the North Pacific Ocean. The back-calculation approach was tested against a known anthropogenic tracer, chlorofluorocarbon-11 (CFC-11), and also by reconstructing an ocean general circulation model's (OGCM) anthropogenic $\delta^{13}C$ change. MIX proved accurate to ±10% against measured CFC-11, but only to ± ∼25% reconstructing the OGCM's $\delta^{13}C$ change from 1992 model output. The OGCM's CFC distribution was also poorly reconstructed using MIX, indicating that this test suffers from limitations in the OGCM's representation of water masses in the ocean. The MIX industrial-era near-surface (200 m) $\delta^{13}C$ change reconstructed from the WOCE P13N data ranged from −0.8‰ in the subtropics (15–30°N), to −0.6‰ in the tropics (10°N), and −0.4 to −0.2‰ north of 40°N. Depth-integrated changes along 165°E were −400‰·m to −500‰·m at low latitudes, and were smaller (−200‰·m) north of 40°N. The MIX North Pacific $\delta^{13}C$ change is consistent with the global anthropogenic CO_2 inventory of 118 ± 17 Pg from ΔC^*.

1. Introduction

Recent developments in techniques for reconstructing anthropogenic CO_2 burdens, notably the ΔC^* approach (Gruber et al., 1996), have been applied in a series of studies to estimate the global oceanic burden of anthropogenic CO_2 (Sabine et al., 2004). A simplification of the ΔC^* approach uses chlorofluorocarbon (CFC) ages to quantify anthropogenic CO_2 accumulation over the past 30 yr (Watanabe et al., 2000). McNeil et al.'s (2003) CFC based global CO_2 uptake rates during 1980–1999 were broadly consistent with estimates based on measured air-sea CO_2 (Takahashi et al., 2002) and $^{13}C/^{12}C$ of CO_2 (Gruber and Keeling, 2001; Quay et al., 2003) disequilibria, and with the recent estimate based on measured atmospheric oxygen and CO_2 changes (Battle et al., 2000). Observations of the recent decline in the $^{13}C/^{12}C$ ratio of oceanic dissolved inorganic carbon (DIC) due to addition of relatively ^{13}C depleted anthropogenic CO_2 (the oceanic ^{13}C Suess effect), have been compiled as an independent means for estimating the ocean's uptake rate of fossil fuel CO_2 over the past few decades (Quay et al., 1992; 2003; Bacastow et al., 1996; Heimann and Maier-Reimer, 1996), and these results have proven globally consistent with the CFC and atmospheric O_2 based estimates.

The global anthropogenic CO_2 changes that have been reconstructed from oceanic DIC data used the ΔC^* approach (Gruber et al., 1996), which relies on an assumption that the ocean-atmosphere CO_2 disequilibrium has remained constant over time. Over much of the low-latitude ocean, this assumption has proven reasonable (within errors) for CO_2 (Matear and

*Corresponding author.
e-mail: rolf@u.washington.edu
DOI: 10.1111/j.1600-0889.2007.00250.x

McNeil, 2003), but because the $^{13}C/^{12}C$ of oceanic DIC (hereafter, $\delta^{13}C$) equilibrates much more slowly with respect to air-sea gas-exchange than does DIC (Broecker and Peng, 1974), this approximation cannot be made when reconstructing ocean $\delta^{13}C$ changes. This means that the contribution to observed trends in preformed $\delta^{13}C$ (Kroopnick et al., 1985) in the ocean interior from mixing among different water masses is more difficult to quantify. Thus back-calculations of the $\delta^{13}C$ change based on present-day data have been performed in only a few locations and, because they rely on CFC dating, are limited to the last 20–30 yr (Sonnerup et al., 1999). Oceanic anthropogenic CO_2 estimates based on ΔC^*, on the other hand, reflect the entire industrial era since before 1800. This difference in timescales has hindered comparison of oceanic $\delta^{13}C$ and $^{12}CO_2$ changes.

Goyet et al. (1999) back-calculated the Indian Ocean's anthropogenic CO_2 change introducing the 'MIX' approach, that departs from the traditional family of reconstructions based on preformed DIC. The MIX approach uses a multiparameter mixing model (Tomczak and Large, 1989) to calculate the relative contributions that a few (basin- or cruise-specific) water-mass end-members make to each water sample. In Goyet et al.'s (1999) application, temperature (T) and salinity (S) were used as conservative parameters and alkalinity and dissolved oxygen (O_2) were used as nonconservative parameters. The mixing model uses each sample's O_2 depletion and alkalinity enrichment relative to its end-member composition to quantify the biological (remineralization) contribution to DIC. In the original MIX approach (Goyet et al., 1999), a history of anthropogenic CO_2 changes in each end-member is approximated as a function of depth from its surface source. The combination of end-members' surface DIC changes and depth penetration scales that best reproduces the present-day DIC distribution at depth is determined iteratively. The 1995 anthropogenic CO_2 inventories along 10°N in the Indian Ocean derived from MIX were about 20% smaller than reconstructed using ΔC^*. Most of the discrepancy occurred in the main thermocline, where the ΔC^* based anthropogenic CO_2 estimates were double the MIX estimates (Coatanoan et al., 2001).

The MIX approach provides one way to reconstruct industrial era ocean $\delta^{13}C$ changes because it does not require that the surface ocean's $\delta^{13}C$ (or DIC) change keep pace with atmospheric changes. The approach explicitly handles mixing among different water masses, each with potentially different responses to the atmospheric $\delta^{13}C$ change, so it can afford broader geographic and depth coverage than is possible using preformed $\delta^{13}C$ (i.e. Sonnerup et al., 1999; Takahashi et al., 2000). Another advantage of the MIX approach is that it does not rely on ^3H-^3He or CFC ages, whose mixing biases may be substantial and difficult to quantify (Waugh et al., 2003), and which limit other $\delta^{13}C$ reconstructions (e.g. Sonnerup et al., 1999) to the past 20–30 yr only.

In this paper, we use MIX to estimate industrial era (1765–1992) $\delta^{13}C$ changes along 165°E in the North Pacific Ocean using $\delta^{13}C$ data from the WOCE P13N line measured in 1992. To quantify the accuracy of the MIX approach, we test its ability to reconstruct the CFC-11 distribution along 165°E, and find that a simple modification to MIX improves both accuracy and computational efficiency. We test this modified MIX approach by reconstructing the industrial era $\delta^{13}C$ changes predicted in an ocean general circulation model (OGCM). Additionally, we use the OGCM to extrapolate the MIX calculated $\delta^{13}C$ change determined for P13N along 165°E to a global ocean industrial era $\delta^{13}C$ change. We use this MIX-derived ocean wide $\delta^{13}C$ change to tentatively estimate industrial era oceanic CO_2 uptake and conclude by making recommendations of the MIX approach's most promising future applications.

2. Data

We used the WOCE P13N $\delta^{13}C$ data collected during September 1992 along 165°E in the North Pacific Ocean (Fig. 1) and analyzed at the University of Washington (Quay et al., 2003) to a precision of ±0.03‰. The P13N CFC data were measured at sea following Bullister and Weiss (1988). Generally, the shipboard CFC-11 measurements had a detection limit of 0.005–0.01 pmol kg^{-1} (1 pmol = 1 picomole = 10^{-12} mole). The precision for the CFC-11 measurements, based on analyses of replicate samples, was estimated to be the greater of 0.01 pmol kg^{-1} or 1% of CFC-11 concentration. This CFC data set also included carbon-tetrachloride (CCl_4) measurements from the same chromatograms. The detection limit for aqueous CCl_4 was ~0.015 pmol kg^{-1}, and the precision of the CCl_4 measurements on this cruise was ~0.02 pmol kg^{-1} or 3% , whichever was greater.

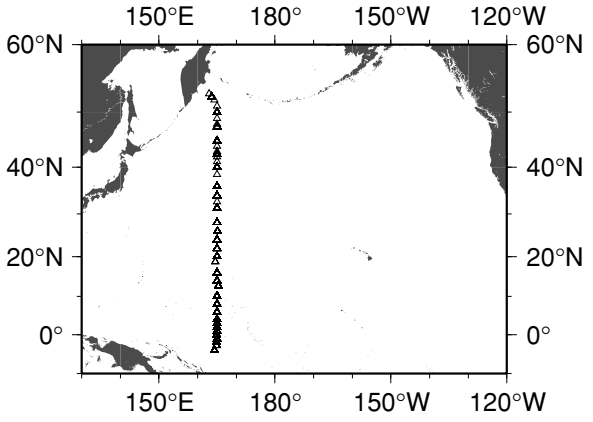

Fig. 1. Station locations during the 1992 WOCE P13N cruise in the North Pacific Ocean.

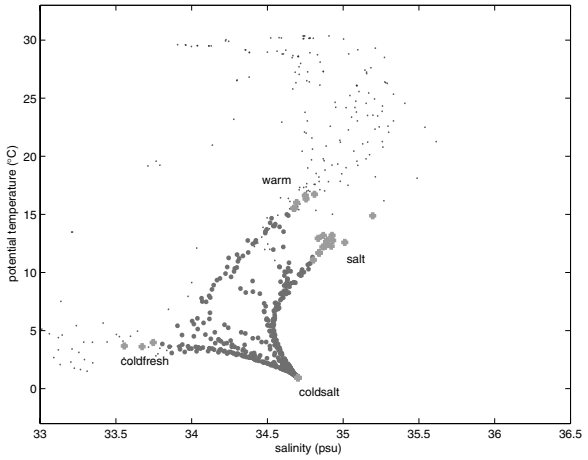

Fig. 2. θ-S diagram from the 1992 WOCE P13N line in the North Pacific Ocean (·). Samples deeper than 200 m only (•) were used in the four end-member (+) MIX calculations.

3. Testing anthropogenic change reconstructions from the MIX approach

3.1. Testing MIX with CFC observations

We evaluated the MIX approach's performance reconstructing a known anthropogenic tracer, CFC-11, along the P13N section. Following Goyet et al. (1999), we identified the deepest wintertime mixed layer along this section, ~200 m, using a 0.125 σ_θ increase criterion and climatological data (Monterey and Levitus, 1997). We then used the potential temperature (θ) and salinity (S) distribution during P13N to select the θ and S characteristics of four end-members deeper than 200 m (Fig. 2). These end-members, selected such that all subsurface (Z > 200 m) samples could be described by their combination, were selected based on the θ-S plot alone. Additionally, we determined, from the mean $\pm 1\sigma$ of the P13N end-member data, the θ, S, nutrient, oxygen, DIC and δ^{13}C characteristics needed for applying the MIX approach to δ^{13}C (Table 1).

Using MIX, the anthropogenic perturbation is not determinable at the sea surface where temperature and salinity are not conservative tracers. Deeper than 200 m, we used extended optimum multiparameter analysis (OMP, Karstensen and Tomczak, 1998) to calculate end-member mixing proportions that, in a least-squares sense, best describe each sample's θ, S, nutrient and oxygen concentrations (Fig. 3). For assumed steady-state tracers, extended OMP analysis represents the P13N measured tracer fields as a combination of mixing between four source water types as follows:

$$\begin{aligned}
&\sum_{i=1}^{4} X_i = 1\\
&\sum_{i=1}^{4} \theta_i X_i = \theta_{\text{measured}}\\
&\sum_{i=1}^{4} S_i X_i = S_{\text{measured}}\\
&\sum_{i=1}^{4} O_{2i} X_i - \Delta O_2 = O_{2\text{measured}}\\
&\sum_{i=1}^{4} PO_{4i} X_i + \Delta O_2 \frac{PO_4}{O_2} = PO_{4\text{measured}}\\
&\sum_{i=1}^{4} NO_{3i} X_i + \Delta O_2 \frac{NO_3}{O_2} = NO_{3\text{measured}}\\
&\sum_{i=1}^{4} SiO_{3i} X_i + \Delta O_2 \frac{SiO_3}{O_2} = SiO_{3\text{measured}}
\end{aligned} \tag{1}$$

Here X_i represents the mixing contribution of each end-member, i, to each water sample. θ_i, S_i, O_{2i}, PO_{4i}, NO_{3i}, and SiO_{3i} are determined from the P13N end-members identified from the P13N θ-S diagram (Fig. 2). The first equation expresses mass conservation, and θ and S are used as conservative mixing parameters. Oxygen (O_2) and nutrients (NO_3, PO_4, and SiO_3) are nonconservative mixing parameters where each mixture's oxygen composition is adjusted for an oxygen consumption term (ΔO_2), and the nutrients (for example NO_3) are corrected by the ΔO_2 terms using constant 'Redfield' remineralization ratios ($NO_3/\Delta O_2$), adopted here from Anderson and Sarmiento (1994). The equations are weighted according to the measurement accuracy and variance of each tracer, and more importantly according to uncertainties in the remineralization ratios. In our application, mass conservation is weighted most heavily, followed by θ and S, O_2, NO_3 and PO_4. SiO_3 does not contribute significantly due to

Table 1. End-member characteristics determined from WOCE P13N along 165°E in 1992, in the North Pacific Ocean. The δ^{13}C of the end-member samples typically differed by < 0.05‰

	θ °C	S	O_2 μmol kg^{-1}	PO_4 μmol kg^{-1}	NO_3 μmol kg^{-1}	Si μmol kg^{-1}	DIC μmol kg^{-1}	$^{\delta 13}$C ‰
Warm	16.1	34.7	203.1	0.3	4.5	5.6	2032	0.81
Salty	12.6	34.9	121.2	1.4	19.5	16.9	2152	0.76
Coldfresh	3.8	33.7	167.7	2.4	33.6	70.7	2227	−0.11
Coldsalt	0.95	34.7	181.1	2.3	32.7	130.0	2285	0.33

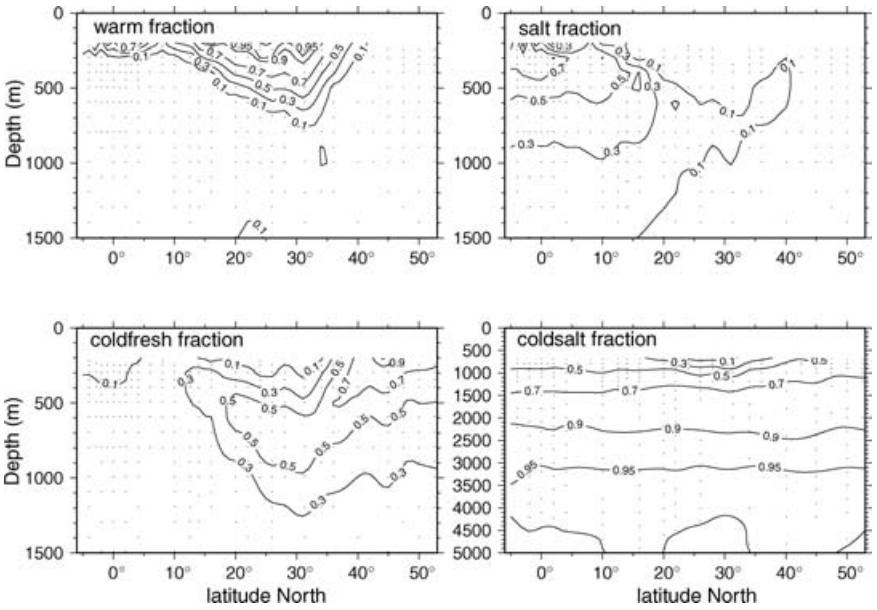

Fig. 3. Latitude-depth distributions of the four end-member water types calculated by extended OMP (Karstensen and Tomczak, 1998) from the 1992 WOCE P13N data in the North Pacific Ocean.

substantial uncertainty in the silicate remineralization ratio. The mixing contributions X_i are determined by solving the system of eq. (1) by nonnegative least squares (Fig. 3).

Because the P13N line spans almost the entire meridional extent of the western North Pacific Ocean, the P13N θ-S diagram is fairly representative of the major North Pacific water masses west of Hawaii (Pickard and Emery, 1990). The 'warm' and 'coldfresh' end-members correspond, both spatially and in terms of their nutrient and θ-S properties, to North Pacific Central Water (NPCW) and North Pacific Intermediate Water (NPIW), respectively, both of which are ventilated within the North Pacific and adjacent seas. The 'coldsalt' end-member corresponds to Pacific Deep Water. The very low natural ^{14}C (Stuiver et al., 1983), high AOU, and absence of bomb-^{14}C (Broecker et al., 1995) and CFCs (Warner et al., 1996) in these waters indicate that these waters are very slowly ventilated, likely bearing little to no anthropogenic CO_2 during the 1990s. The 'salt' end-member corresponds spatially and by its nutrient and θ-S properties with the Pacific Equatorial Water described by Pickard and Emery (1990). This water mass occurs at highest density within the equatorial undercurrent and associated eastward currents within 5° of the equator at 165°E. The core of this end-member does not appear to be ventilated directly along the P13N section (Fig. 3). These waters likely obtained any anthropogenic tracers via air-sea exchange in their formation regions in the eastern South Pacific Ocean (35°–45°S) (Huang and Qiu, 1998; Johnson and McPhaden, 1999), and via mixing along their pathway to the equatorial Pacific Ocean at 165°E. The northern limb of the subsurface countercurrent along 165°E bears some contribution from low salinity North Pacific waters as well (Johnson and McPhaden, 1999).

For tracers that have undergone an anthropogenic change, the MIX approach seeks a depth-functionality of that change in each end-member i. We estimated the 1992 CFC distribution by seeking, for each of the four end-members, a CFC increase at the near-surface (200 m), and a depth attenuation of that increase, that best reproduces the 1992 CFC measurements. To correct for the stronger temperature dependence of CFC solubility relative to that of $\delta^{13}C$, we used CFC saturation levels relative to the 1992 atmosphere (Fig. 4) calculated from the CFC concentration data (Warner and Weiss, 1985). In the original MIX approach, Goyet et al. (1999) used 'Sigmoid functions' to describe the depth penetration of DIC changes within each end-member component:

$$\Delta ANT_i^{\text{sample}}(Z) = \Delta ANT_i^{sfc} - \frac{1}{\left[1 + e^{-S_i(Z - Z_i^{\circ})}\right]^{A_i}} \tag{2}$$

where ΔANT_i^{sfc} is the anthropogenic change at 200 m in the ith end-member, Z_i° is the penetration depth of the (200 m) maximum change, S_i is the inverse e-folding depth scale of the attenuation of this maximum change below Z_i°, and A_i describes the asymmetry of the sigmoid (Goyet and Davis, 1997). Each end-member's anthropogenic imprint has four degrees of freedom using this formalism.

We modified the MIX approach by calculating the attenuation of the anthropogenic signal below 200 m as a linear function of potential density:

$$\Delta ANT_i^{\text{sample}}(\sigma_\theta) = \Delta ANT_i^{sfc} \cdot \left\{1 - \frac{{\sigma_\theta}^{\text{sample}} - {\sigma_\theta}_i^{\text{end\_member}}}{{\sigma_\theta}_i^{\circ} - {\sigma_\theta}_i^{\text{end\_member}}}\right\} \tag{3}$$

where ${\sigma_\theta}^{\circ}$ is the potential density where the anthropogenic change vanishes for each end-member i. When ${\sigma_\theta}^{\text{sample}} <$

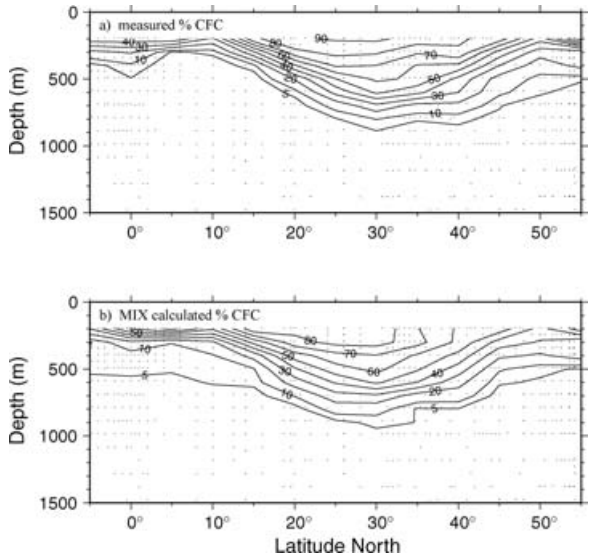

Fig. 4. The percent CFC-11 saturation relative to the atmosphere measured during the 1992 WOCE P13N cruise along 165°E in the North Pacific Ocean (a) and calculated from the MIX model's best-fit combination (using eq. 3) of end-member CFC saturation levels and penetration densities (b).

$\sigma_\theta{}^{\text{end-member}}$, the end-member's change is set equal to its maximum change. This modified MIX approach has only two degrees of freedom per end-member: the near-surface change, ΔANT_i^{sfc}, and the maximum penetration density ($\sigma_{\theta i}^{\circ}$), and is consistent with the idea that along-isopycnal ventilation is the dominant process ventilating anthropogenic tracers into the North Pacific Subtropical thermocline (Michel and Suess, 1975; Fine et al., 1981; Warner et al., 1996). In the P13N measurements, CFC saturation levels >10% were linearly related to potential density.

For each subsurface sample we used the OMP mixing coefficients and assigned contributions of CFC from each end-member, for all possible combinations of free parameters in both the depth- (eq. 2) and density- (eq. 3) dependent formalisms, to calculate CFC saturation levels. For each free parameter, a wide range of possible values was permitted, and discrete variations within these ranges were tested (Table 2). The free parameters were varied systematically and independently, for each end-member.

The combination of parameters that yielded the least-squares fit to the data was taken as the most likely to describe the anthropogenic CFC burden (Fig. 4). The depth- and density-dependent MIX estimates are similar in upper waters where CFC saturation levels are >50%. Residuals (Fig. 5) from the depth-dependent sigmoid functions (eq. 2) were typically ±6.5% CFC saturation, and were somewhat smaller, ±4.7%, and were normally distributed with respect to depth using density dependence (eq. 3). Residuals from predicting CFC at depth were comparable to the scatter in the CFC saturation level measured in the P13N end-member samples (typically ±6%), so refinements in the attenuation functions are unlikely to improve the CFC reconstruction.

The MIX reconstruction provides a fair representation of the CFC distribution along this section (Fig. 4). The signal-to-noise ratio (S/N) of the MIX CFC determination, that is, the observed

Table 2. Near-surface changes and penetration function parameters used to calculate the CFC change

Parameter	Range	Step size	Best fit (least squares)
Sw	10^{-4} to 2.5	0.05	2.0
Ss	10^{-4} to 2.5	0.05	2.0
Scf	10^{-4} to 2.5	0.05	0.1
Scs	10^{-4} to 2.5	0.05	See notes[1]
Δw	0 to 110%	2.5%	85%
Δs	0 to 110%	2.5%	70%
Δcf	0 to 110%	2.5%	30%
Δcs	0 to 25%	1%	0%
Zw	200 to 1000 m	25 m	600 m
Zs	200 to 1000 m	25 m	200 m
Zcf	200 to 1000 m	25 m	700 m
Zcs	200 to 5500 m	250 m	See notes[1]
P13N using Linear Density Functions			
Δw	0 to 110%	2%	88%
Δs	0 to 110%	2%	16%
Δcf	0 to 110%	2%	54%
Δcs	0 to 110%	2%	0%
$\sigma_\theta{}^\circ$w	25.51 to 28.9 σ_θ	0.1 σ_θ	28.4 σ_θ[2]
$\sigma_\theta{}^\circ$s	26.4 to 28.9 σ_θ	0.1 σ_θ	26.6 σ_θ
$\sigma_\theta{}^\circ$cf	26.73 to 28.9 σ_θ	0.1 σ_θ	27.25 σ_θ
$\sigma_\theta{}^\circ$cs	up to ∞	0.1 σ_θ	∞

[1]The coldsalt end-member's best-fit CFC saturation level was zero.
[2]The best-fit warm end-member's CFC change attenuates primarily by dilution (Fig. 3).

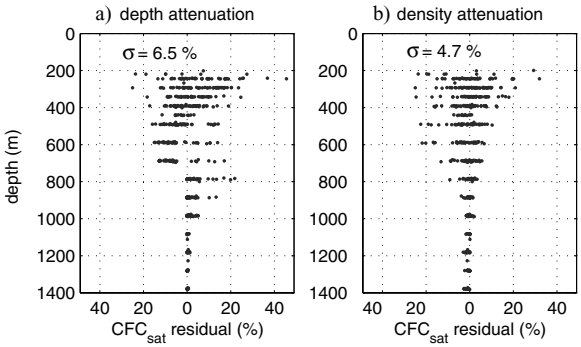

Fig. 5. Residuals (measured–MIX) of MIX's CFC-11 saturation levels assuming depth-dependent (a) and density-dependent (b) attenuation of the anthropogenic signal.

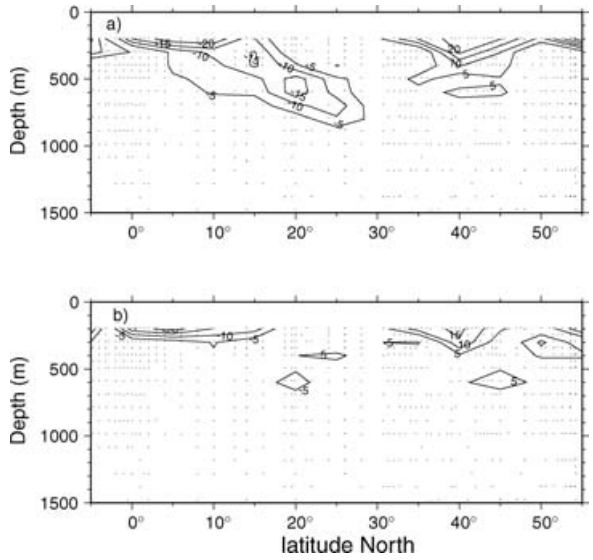

Fig. 6. Residuals (measured–MIX) of density-dependent (a) and density and latitude dependent (b) MIX models' least-squares fit to the CFC saturation levels measured during the 1992 WOCE P13N cruise along 165°E in the North Pacific Ocean.

CFC saturation level divided by the MIX prediction's error was, generally, >10 throughout the upper 1000 m. There were systematic spatial patterns in the residuals, however (Fig. 6). There was no corresponding pattern in residuals from predicting T (or S) using the OMP mixing model, indicating that the CFC residual pattern likely reflected the limitations of the anthropogenic component of MIX. In the density-dependent MIX model, the CFC change was overestimated by ∼10% CFC saturation in the depth range 300–700 m from 10°–25°N and underestimated by about 10–20% CFC saturation from 35°–45°N shallower than 400 m (Fig. 6). North of 30°N, the density-dependent approach was fairly accurate at lower CFC saturation levels found at depth (Z > 400 m). The best-fit CFC saturation maxima of 88% and 16% for the 'warm' and 'salt' end-members, respectively, agreed well with those measured in the P13N end-members (84 ± 6% and 20 ± 6%, respectively). The MIX maximum CFC change for the 'coldfresh' end-member (30%) was lower than measured (53 ± 15%), however.

The density-dependent MIX residuals were highest (+30% CFC) where the North Pacific Intermediate Water (NPIW) concentrations were highest, and were most negative (−15% CFC) where the southward NPIW intrusion attenuates to <0.3 (Fig. 3). In this end-member's geographic range, MIX CFC levels were too large in the subtropics and too small at higher latitudes (>35°N) because MIX minimized residuals over the entire section. In this case MIX attenuated the end-members' changes along an isopycnal surface by dilution only (Fig. 3), thus requiring near-outcrop changes that were too small to minimize overprediction of the subtropical change. A simple solution would be to also attenuate the anthropogenic change as a function of

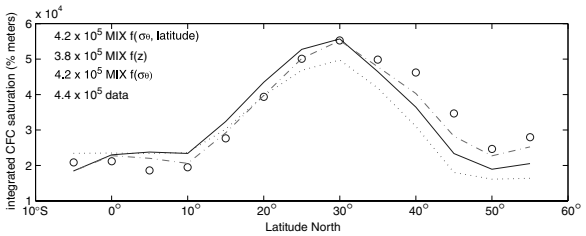

Fig. 7. The depth-integrated CFC-saturation measured (◯) and calculated using the MIX approach's depth-dependent (····), density-dependent (- - -), and density- and latitude-dependent (-·-·-) attenuation formalisms.

distance from the end-member:

$$\Delta ANT_i^{\text{sample}}(\sigma_\theta) = \Delta ANT_i^{sfc} \cdot \left\{1 - \frac{\sigma_\theta^{\text{sample}} - \sigma_{\theta i}^{\text{end\_member}}}{\sigma_{\theta i}^{\circ} - \sigma_{\theta i}^{\text{end\_member}}}\right\} \times \left\{1 - \frac{lat_i^{\text{end\_member}} - lat^{\text{sample}}}{lat_i^{\circ} - lat_i^{\text{end\_member}}}\right\} \quad (4)$$

where $lat_i^{\text{end\_member}}$ is the maximum concentration latitude (Fig. 3) of the ith end-member, lat_i° is the latitude where the anthropogenic change attenuates to zero, and lat^{sample} is the sample location. Since no significant residual patterns corresponded to the other three end-members, the calculations were repeated using eq. (3) for these end-members, and eq. (4) for the 'coldfresh' end-member.

When latitude-dependent attenuation was added, the residual sum-of-squares decreased by a factor of ∼2, and the residuals were on the order of ±3.4% CFC saturation. The shallow (200–400 m) under prediction from 30–45°N was improved and the over prediction at 10–25°N was corrected (Fig. 6). MIX still under predicted the shallow (200–300 m) CFC levels at 35°–45°N, and over predicted it in the tropics (0°–15°N). However, latitude dependence improved the depth-integrated CFC burden along this section, to within 8% of observed, while the density and depth only formalisms were too low by 16% and 20%, respectively (Fig. 7). In general, the MIX tests on the measured CFC distribution indicate a promising degree of accuracy in reconstructing anthropogenic changes (Figs. 4 and 7).

3.2. *Testing MIX using an ocean circulation model*

The anthropogenic δ^{13}C perturbation has occurred over a longer (∼200 yr) timescale than has the CFC transient (∼50 yr), and MIX δ^{13}C reconstructions include biological corrections that are absent in the MIX CFC calculations. To address these limitations we tested MIX's ability to reconstruct industrial era δ^{13}C changes that were simulated in an ocean general circulation model (OGCM) between 1765 and 1992 by using the OGCM's 1992 output only. The model was Modular Ocean Model, Version 3 (Pacanowski and Griffies, 1999) on a 4° by ∼4° grid with 24 vertical levels ('MOM-3'). This version included a

Table 3. The fractionation $\epsilon = (\delta^{13}C_{org} - \delta^{13}C_{DIC})$ during formation of organic matter estimated from the difference between zonally averaged δ^{13}C of DIC in surface waters (Quay et al., 2003) and δ^{13}C of surface water particulate organic matter (Goericke and Fry, 1994)

Latitude Band	$\epsilon(\delta^{13}C_{org} - \delta^{13}C_{DIC})$
20°N–65°N	−22.6‰
Equator–20°N	−21.3‰
40°S–equator	−22.1‰
50°S–40°S	−23.8‰
60°S–50°S	−27.9‰
South of 60°S	−30.2‰

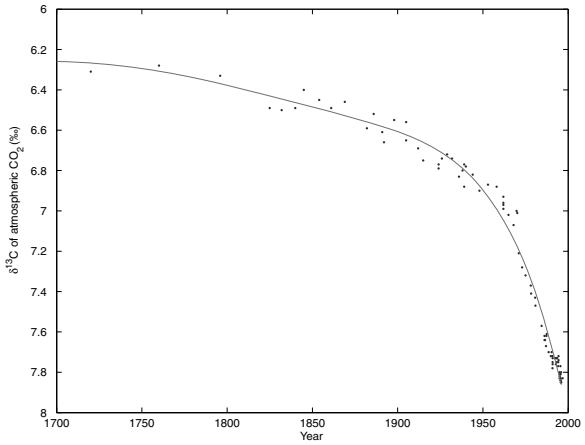

Fig. 8. The atmospheric δ^{13}C history derived from ice core, firn, and air measurements (·) (Francey et al., 1999) and used to force the geochemical ocean general circulation model (—).

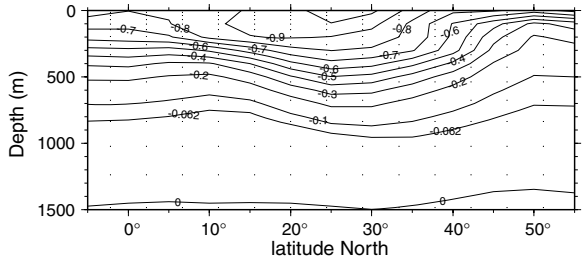

Fig. 9. The 1765–1992 δ^{13}C change (‰) simulated by the OGCM along 165°E in the North Pacific Ocean.

Gent-McWilliams (1990) mixing scheme, was driven by climatological winds (Hellerman and Rosenstein, 1982), with vertical mixing in the upper ocean set at 0.15 cm^2 s^{-1}, and isopycnal mixing set at 1000 m^2 s^{-1}. A geochemical model that calculates biological production by restoring ($\tau = 30$ days) sea-surface PO_4 levels to seasonal climatological data (Conkright et al., 1994) using a 'Redfield' C:P ratio (Anderson and Sarmiento, 1994) was included. A more complete description of this geochemical ocean model (the 'PRINCE' model in OCMIP-2) can be found in Gnanadesikan et al. (2002, their version KVLOW+AILOW) and its uptake of anthropogenic CO_2 in Orr (2002) and Matsumoto et al. (2004).

We added ^{13}C to the OCMIP geochemical cycling scheme. Temperature-dependent fractionation during air-sea exchange of CO_2 and between DIC species were calculated following Zhang et al. (1995). Fractionation during organic matter formation was calculated from the difference (ε) observed between sea surface δ^{13}C of DIC and particulate organic matter (Table 3), while calcium carbonate formed was 1‰ enriched relative to DIC (Bonneau et al., 1980). The model assumed that no $^{13}C/^{12}C$ fractionation occurred during remineralization of organic matter and dissolution of calcium carbonate.

The general circulation model's $^{13}CO_2$ and $^{12}CO_2$ fields were equilibrated (∼15,000 model years) with the pre-industrial atmosphere, 278 ppm CO_2 and $\delta^{13}C = -6.28$‰ (Francey et al., 1999) for 1765. The model was then forced with the atmospheric pCO_2 history from a smoothing spline fit through the Siple ice core and Mauna-Loa CO_2 records (Orr, 2002). The temporal evolution of the δ^{13}C of atmospheric CO_2 (Fig. 8) was taken from a spline fit through the Law Dome, Antarctica, ice core and firn record augmented by the Cape Grim air archive after 1978 (Francey et al., 1999). In this record, the atmospheric δ^{13}C decrease to 1992 was −1.54‰.

The model's surface water δ^{13}C change (Fig. 9) along the 165°E section was −0.9 to −1.0‰ in the subtropics (15–35°N), −0.8‰ at the equator and −0.6‰ in the subpolar region (∼50°N). The 1992 ^{13}C Suess effect was detectable (−0.06‰, approximately twice the precision of δ^{13}C measurements) down to about 850 m throughout the North Pacific along this section in this model simulation.

Next we attempted to back-calculate the model's δ^{13}C change (Fig. 9) using the density-dependent MIX approach and the 1992 model output. Based on the θ-S plot from the model's 165°E section (Fig. 10), four end-member distributions were calculated using extended OMP, as outlined above. The OGCM's prominent end-members (Fig. 11) are spatially distributed in a fashion similar to the WOCE P13N end-members (Fig. 3). For each grid point, the mixture's preformed DIC (*DIC°*) was calculated by subtracting the difference between the alkalinity measured and the alkalinity calculated from the end-member mixture, and subtracting any DIC added by organic matter remineralization, estimated from the difference (ΔO_2) between the O_2 measured and the end-member mixture's O_2:

$$\mathrm{DIC}^{\circ} = \mathrm{DIC}^{\mathrm{measured}} - \left(\frac{\mathrm{C}}{\mathrm{O}_2}\right) \cdot \Delta \mathrm{O}_2 - \frac{1}{2}\left[ALK^{\mathrm{measured}} - ALK^{\mathrm{mixture}} + \left(\frac{\mathrm{N}}{\mathrm{O}_2}\right) \cdot \Delta \mathrm{O}_2\right]. \quad (5)$$

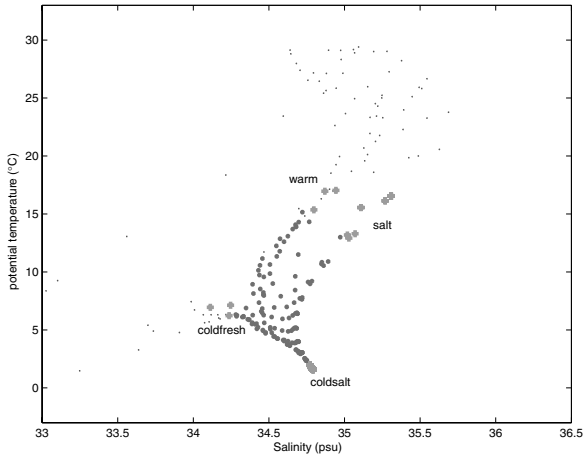

Fig. 10. The OGCM's θ-S distribution along 165°E in the North Pacific Ocean (·). Samples deeper than 200 m only (•) were used in the four end-member (+) MIX calculations.

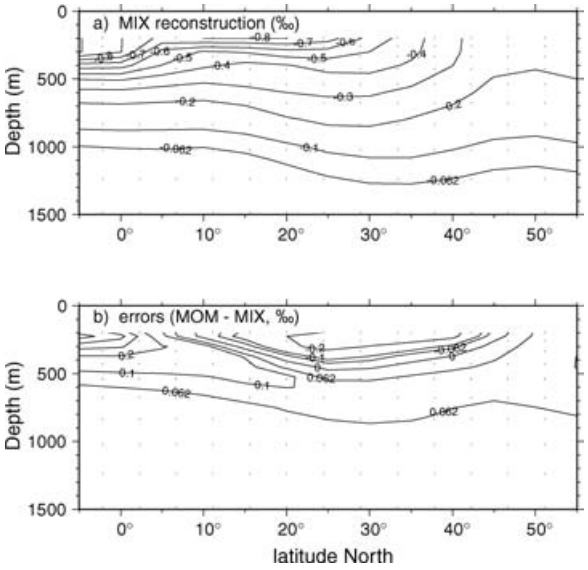

Fig. 12. The anthropogenic δ^{13}C change along 165°E in the OGCM reconstructed using the 1992 model output and the density-dependent (eq. 3) MIX approach along 165°E in the North Pacific Ocean (a), and the difference between the OGCM's δ^{13}C change and that back-calculated using MIX (b).

Here C/O_2 and N/O_2 are 'Redfield' ratios of organic matter remineralization (Anderson and Sarmiento, 1994), and ΔO_2 are oxygen depletion relative to the end-member mixture determined by OMP. We similarly calculated preformed δ^{13}C (Kroopnick, 1985) using the OGCM's δ^{13}C of marine organic matter. Because formation and dissolution of calcium carbonate is not an important driver of oceanic δ^{13}C, we neglected alkalinity changes when determining preformed δ^{13}C (i.e. Sonnerup et al., 1999). Finally, the near-surface δ^{13}C changes and penetration densities and depths yielding the least-squares fit to the 1992 model output were identified iteratively, as outlined for CFCs above, and described in detail for the WOCE P13N δ^{13}C below.

The MIX model did a fair job calculating the OGCM's 1992 δ^{13}C values. MIX residuals were everywhere <0.1‰, and were typically <0.06‰. However, the MIX reconstruction of the OGCM's δ^{13}C change (Fig. 12) only roughly approximated the

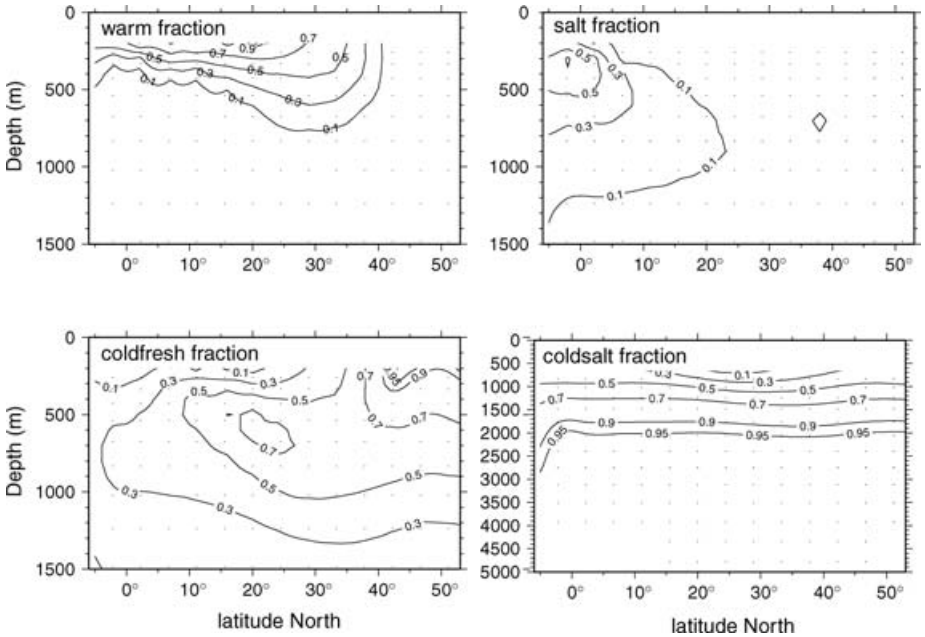

Fig. 11. Latitude-depth distributions of the four end-member water types calculated from the OGCM output using OMP (Karstensen and Tomczak, 1998) along 165°E in the North Pacific Ocean.

OGCM's simulated δ^{13}C change (Fig. 9). Near-surface (200 m) δ^{13}C changes in the MIX reconstruction were accurate to within 10–30% throughout the subtropics (10°–40°N), but were significantly smaller throughout the subpolar region (−0.32‰, instead of −0.55‰, at 40°N, for example). In the tropics, the MIX near-surface δ^{13}C change was significantly larger than in the OGCM (−1.0‰, instead of −0.65‰, at the equator). The maximum penetration depth of the Suess effect (−0.06‰) from MIX (1100–1200 m) was significantly deeper than in the forward model results (∼850 m). The S/N of the MIX determination of the OGCM's δ^{13}C change was ∼2–3 from 600–800 m and better, ∼6–10, from 200–600 m.

The MIX predicted depth-integrated δ^{13}C changes were too large relative to the model results. MIX calculations using depth-dependent (eq. 2) or density and latitude dependence (eq. 4) did not improve the situation. In the subpolar region, individual MIX δ^{13}C change isopleths are ∼300 m deeper than corresponding changes in the OGCM. The MIX-predicted depth-integrated δ^{13}C change was generally more uniform meridionally than the model predictions. This lack of spatial structure may be due to MIX's inability to account for more than four water masses, whereas the real (and model) ocean circulation is likely more complex. For example, we noted that in the tropics MIX overestimates δ^{13}C changes substantially. MIX correctly predicts a large near surface δ^{13}C change in the subtropics (Fig. 9) by assigning a large δ^{13}C change in its 'warm' end-member. This would tend to over predict the tropical δ^{13}C change because the 'warm' end-member occurs at high concentrations at ∼200 m almost to the equator (Fig. 11). Overall, the results using MIX to back-calculate the OGCM's δ^{13}C change tell quite a different story than our test of MIX using P13N CFC data, where MIX proved to be quite accurate.

The 'salt' fraction is relatively less important in MOM, penetrating to only 20°N along the 165°E section (Fig. 11), while it is present throughout the lower subtropical thermocline in the P13N OMP results (Fig. 3). In addition, MOM's 'warm' end-member (North Pacific Central Water) is present at high concentration (>80%) only south of 20°N, while in the P13N data this water mass is significant to ∼35°N. Because these two water masses are of diminished importance in the OGCM's 165°E section, the subtropical thermocline is dominated by one end-member, 'coldfresh' (Fig. 11). The task of accurately representing the OGCM's subtropical δ^{13}C or CFC distribution then relies almost entirely on the parameterization of the perturbation within this end-member. In the P13N CFC-11 reconstruction, the MIX representation of the subtropical tracer burden relies both on the end-member attenuation scheme and on mixing/dilution among the three end-members present in significant amounts in the subtropical thermocline (Fig. 3). It may be the case that because MIX applied to the MOM output represents the subtropics with (mostly) one end-member, it tends to over predict the δ^{13}C perturbation in the lower thermocline and under predict it in the 'coldfresh' outcropping region, an exaggerated analog

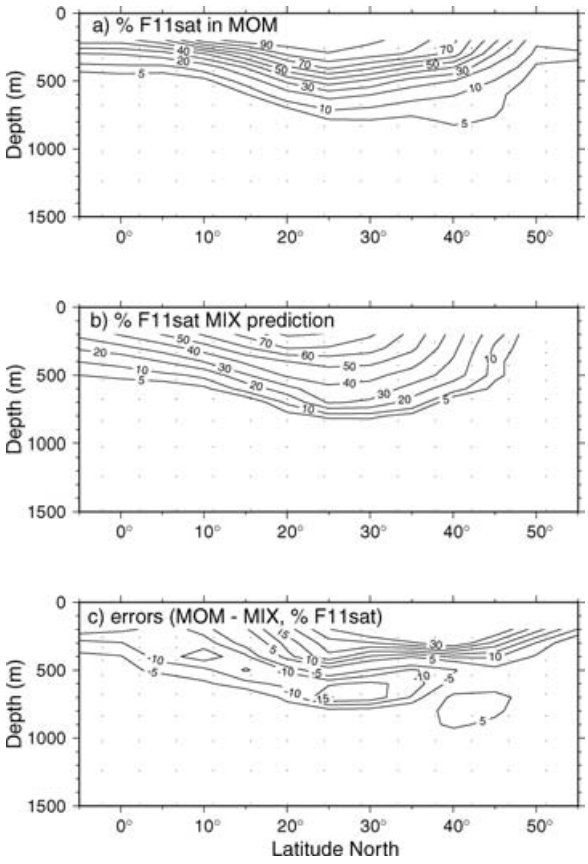

Fig. 13. 1992 CFC-11 saturation levels (%) relative to the atmosphere in the OGCM (a), reconstructed by the density-dependent MIX approach (eq. 3) applied to the OGCM 1992 output (b), and residuals (OGCM output–MIX result) from the MIX reconstruction of the Ocean model's CFC (c) along 165°E in the North Pacific Ocean.

to the situation described for the 'coldfresh' end-member's CFC simulation of the P13N data. However, addition of latitude dependence did not measurably improve the MIX least-squares fit in reconstructing anthropogenic changes within the GCM.

Although the OGCM back-calculation is an internally self-consistent test, we evaluated the possibility that the OGCM may not represent real-world circulation and δ^{13}C changes well enough to fairly evaluate the MIX approach's skill. We did this by comparing MIX reconstructions of the OGCM's CFC field along 165°E in 1992 (Fig. 13) with the MIX P13N CFC reconstruction (Fig. 4). MIX's fit to the model CFC output (Fig. 13) was not as good as for the measured CFC data from P13N (Fig. 6). MIX's near-surface CFC changes were significantly (by >20% CFC saturation) too small throughout the subtropical and subpolar regions, and too large, (by 10% CFC saturation), in the tropics. MIX CFC levels were too low at shallow depths (Z < 400 m), and too high deeper than 500 m (Fig. 13). The S/N for the MIX reconstruction of the OGCM's CFC field was ∼4–7 from 200–600 m, and ∼1 deeper than 600 m. For comparison, MIX proved to be more accurate when applied to

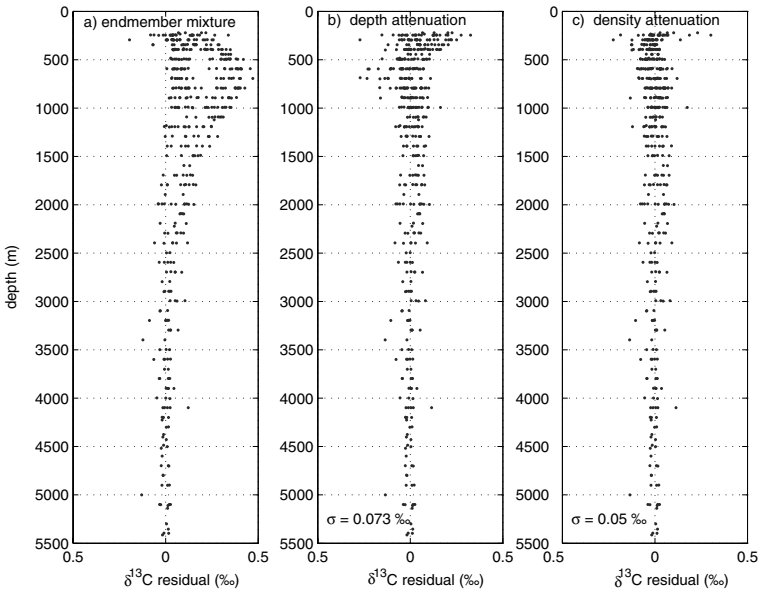

Fig. 14. Differences (residuals) between δ^{13}C measured during WOCE P13N and the OMP mixing model's calculated δ^{13}C when the 1992 average values in the water mass end-members (Fig. 2) were used (a), when the end-members were adjusted for anthropogenic changes as a function of depth (b), and as a function of density (c). Uncertainties represent the scatter ($\pm 1\sigma$) in the residuals.

the P13N CFC data, where the MIX S/N was >10 throughout the upper 1000 m. Thus, the MIX reconstruction of this OGCM's δ^{13}C output likely significantly overstated errors expected from applying the MIX approach to the δ^{13}C data from P13N. We speculate that errors in applying MIX to the P13N δ^{13}C data likely lie between the extremes indicated by the P13N CFC observations, ($\pm$10% of the signal) and by the MIX test on the 165°E OGCM ^{13}C changes ($\pm$25%–50% of the signal) in the upper 1000 m. It is also important to note that the $\pm 1\sigma$ scatter in the MIX model's residuals was usually smaller than, and was thus not an accurate indicator of, uncertainties estimated by tests on known anthropogenic tracer fields.

4. Reconstructing anthropogenic δ^{13}C changes along WOCE P13N

Having a rough uncertainty estimate in hand, we turn to reconstructing the real ocean's anthropogenic δ^{13}C change from the WOCE P13N δ^{13}C data. First, for each P13N data point we calculated preformed DIC (eq. 5) and preformed δ^{13}C (Kroopnick, 1985), as outlined above, using an observed δ^{13}C for marine organic matter of -21‰ (Goericke and Fry, 1994). We then used the OMP mixing coefficients (Fig. 3) and the DIC and δ^{13}C of the end-members (Table 1) determined from the P13N data to calculate the subsurface δ^{13}C distribution that would result if the end-members' anthropogenic signal did not attenuate with respect to depth (Fig. 14). Near-surface (200 m) waters' ^{13}C were fairly well approximated by the end-member mixture (Fig. 14). Between 200 and 2000 m, however, δ^{13}C values calculated from the uncorrected end-member mixtures are lower (by up to 0.5‰) than measured (Fig. 14a), because waters in this depth range bear a smaller anthropogenic δ^{13}C imprint than do the near surface waters used to calculate the δ^{13}C mixture. Deep (>2000 m) δ^{13}C values from the end-member mixture agree with those measured because the dominant end-member in this depth range likely bears no ^{13}C Suess effect. To calculate the anthropogenic δ^{13}C change, we sought the combination of near-surface δ^{13}C changes and density- and depth- penetration length scales that best described, in a least-squares sense, the 1992 δ^{13}C measurements overall (Table 4). Similar to the situation for CFC-11, residuals resulting from the density-dependent (equation 3) function (σ =0.05‰) were smaller than from the depth-dependent (equation 2) sigmoid function (σ =0.07‰, Fig. 14).

The MIX calculated industrial era near-surface δ^{13}C change was approximately -0.8‰ in the Subtropics (15°–30°N), and was smaller (approximately -0.3‰) in the subpolar gyre (Fig. 15). The δ^{13}C change was detectable ($\pm$0.06‰) down to about 1300 m north of 25°N, and down to about 1000 m in the tropics. Residuals from the best-fit density-dependent MIX model (Fig. 15) imply that MIX underestimated the Suess effect in the lower subtropical thermocline (20°–40°N, 500–1000 m), by ~0.05‰, however residuals alone do not necessarily reflect the accuracy of the reconstruction, as discussed above.

We used CCl_4 as a rough gage of MIX's accuracy at depth. Despite its nonconservative behavior, CCl_4 provides a useful tracer for anthropogenic CO_2 and δ^{13}C: any waters tagged with CCl_4 are likely to also carry an anthropogenic CO_2 or δ^{13}C change (Wallace, 1995). In the subtropical and subpolar regions, the δ^{13}C change penetration depth is similar to CCl_4's (Fig. 16), despite the somewhat longer time history of the atmospheric $^{13}CO_2$ perturbation (~200 yr) relative to that of CCl_4 (~100 yr). However, only about 20% of the atmospheric δ^{13}C decrease to 1992 had occurred by the 1890s (Fig. 8), when CCl_4 was

Table 4. Near-surface change and penetration function parameters used to calculate the P13N δ^{13}C change

Parameter	Range	Step size	Best fit (least-squares)
Sw	0.0001 to 2.0	0.01	0.11
Ss	0.0001 to 2.0	0.01	0.01
Scf	0.0001 to 2.0	0.01	1.9
Scs	0.0001 to 2.0	0.01	See notes[a]
Δw	0 to -1.4‰	-0.05‰	-0.85‰
Δs	0 to -1.4‰	-0.05‰	-1.0‰
Δcf	0 to -1.4‰	-0.05‰	-0.1‰
Δcs	0.1 to $-$ 0.1‰	-0.025‰	0.025‰
Zw	200 to 1000 m	50 m	650 m
Zs	200 to 1000 m	50 m	200 m
Zcf	200 to 1000 m	50 m	200 m
Zcs	200 to 5500 m	250 m	5500 m
P13N using Linear Density Functions			
Δw	0 to -1.4‰	-0.05‰	-0.8‰
Δs	0 to -1.4‰	-0.05‰	-1.2‰
Δcf	0 to -1.4‰	-0.05‰	-0.3‰
Δcs	0.04 to -0.04‰	-0.01‰	0.0‰
σ_θ°w	up to 27.9 σ_θ	0.05 σ_θ	27.65 σ_θ
σ_θ°s	up to 27.9 σ_θ	0.05 σ_θ	27.4 σ_θ
σ_θ°cf	up to 32 σ_θ	0.05 σ_θ	28.75 σ_θ
σ_θ°cs	up to ∞	0.1 σ_θ	∞

[a]The best-fit penetration depth for the Coldsalt end-member's δ^{13}C change reached the ocean bottom.

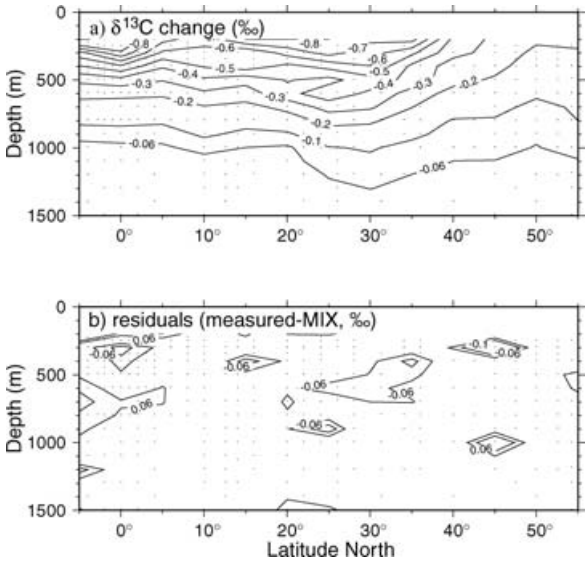

Fig. 15. The total (preindustrial—1992) δ^{13}C change along 165°E in the North Pacific Ocean reconstructed using the MIX approach with density dependent attenuation of the 200 m perturbation in each end-member (a), and residuals (measured–MIX) from the MIX prediction (b).

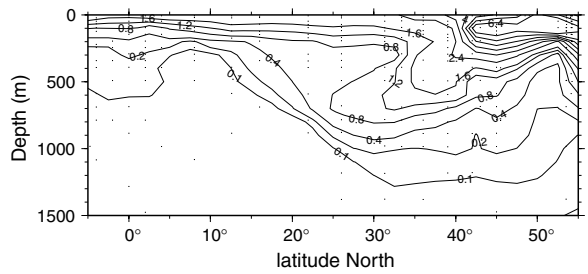

Fig. 16. CCl_4 (pmol kg^{-1}) measured along 165°E in 1992 during the WOCE P13N expedition in the North Pacific Ocean.

introduced into the atmosphere. In the tropics (5°S–10°N) the industrial era δ^{13}C changes (Fig. 15) penetrate much deeper (∼1000 m at 10°N) than CCl_4 in 1992 (∼500 m). This mismatch is likely due to a MIX overestimate of the δ^{13}C change, and not to in-situ degradation of CCl_4, since CCl_4 is approximately conservative at the cold temperatures found at depth (Huhn et al., 2001).

On the P13N section, the anthropogenic signal in the end-member corresponding to North Pacific Intermediate Water (NPIW, 'coldfresh' in Fig. 3) was weakly constrained. For example, in an alternate scenario yielding only a slightly larger sum-of-squares and identical scatter, ±0.049‰, the total δ^{13}C change was ∼15% larger in near-surface (∼200 m) waters north of 30°N, and in the lower thermocline (500–1000 m) individual δ^{13}C change contours north of 20°N were ∼250 m deeper than in the least-squares scenario. These differences are within the range of uncertainties estimated from the CFC and GCM δ^{13}C reconstructions. The best-fit δ^{13}C changes in the other two shallow end-members were not affected by the coldfresh end-member uncertainty. The subtropical and tropical end-members' changes were better constrained, i.e. a small change in either resulted in a substantial increase in the magnitude of the residuals.

The MIX δ^{13}C change was sensitive to the δ^{13}C of organic matter used to calculate preformed δ^{13}C. For example, using a more depleted value of -22‰ yielded a δ^{13}C change that was ∼10% smaller, and using -20‰ yielded a ∼10% larger δ^{13}C change. The residual sum-of-squares was significantly smaller using -21‰, however. This is consistent with Takahashi et al.'s (2000) estimate of –21 ±1‰ based on preformed δ^{13}C in the deep ($\sigma_\theta > 27.7$) North Pacific. In the Southern Ocean a strong meridional trend in the δ^{13}C of particulate organic matter is observed (Goericke and Fry, 1994; Fry et al., 1998), decreasing from approximately -21‰ at 40°S to <-26‰ south of 60°S. In water masses south of 40°S, assuming a δ^{13}C of organic matter that is too ^{13}C enriched would cause an overestimate of the δ^{13}C change on the order of 25% in that end-member component. These errors are small along the P13N section because the

anthropogenic signal was negligible in deep waters, but will certainly need to be considered when applying MIX to reconstruct ocean δ^{13}C changes in the southern hemisphere.

The MIX approach requires that a number of *a-priori* parameters be assigned and subjective choices made. For example, the 'best-fit' MIX solution could be defined variously as the least-squares solution (as presented here), or the solution minimizing the residual scatter, or where the residual weighting is adjusted to prioritize accuracy in the upper/lower thermocline. Any of these could be argued to provide a 'best fit'. We compared the MIX solution from a number of different error minimization criteria, including those listed here, and found that their best-fit solutions do not differ significantly from our least-squares estimate within the uncertainty bounds we estimated, ±10–20% in the upper 500 m, and ±25–30% below.

Use of canonical Redfield ratios (i.e. Redfield et al., 1963) based on an assumed stoichiometry of plankton, rather than the ratios determined from O_2/DIC trends in the ocean interior (Anderson and Sarmiento, 1994) we used here, did make a difference in the anthropogenic δ^{13}C change from MIX, because it changed the proportion of remineralized organic carbon contributing to samples at depth (eq. 5). The end-member distributions (Fig. 3) did not change substantially. The Redfield et al. (1963) O_2/C ratio of 1.30 yielded δ^{13}C changes that were ∼10% smaller at 200 m, agreed with the Anderson and Sarmiento (1994) -based δ^{13}C changes at 400 m, and were ∼25% higher in the lower thermocline (600–800 m). The Anderson and Sarmiento (1994) ratio (O_2/C = 1.45) yielded a far smaller residuals sum-of-squares, however, consistent with the fact that these ratios were determined from O_2 and DIC trends measured in the ocean interior.

The MIX δ^{13}C change results were relatively insensitive to subjective decisions made when determining end-members, and to uncertainties in their characteristics. The end-member choices themselves, limited in any one MIX calculation to four (five, if potential vorticity is included as a tracer), would depend critically on the regional coverage afforded by the data set such that the major water masses present along a cruise section are represented in the OMP mixture. The P13N θ-S and water mass structure (Fig. 2) did not provide any obvious alternate end-member scenarios, although the MIX results' sensitivity to alternate end-member combinations should certainly be considered in future applications.

The MIX near-surface δ^{13}C change along P13N increases equator ward (Fig. 15). The δ^{13}C change is expected to be larger in the subtropics, where waters' residence times at the surface are relatively long, than at subpolar latitudes, where upwelling and overturning prevents surface waters from keeping pace with the atmospheric δ^{13}C change (Quay et al., 1992, Bacastow et al., 1996). However, one prominent feature in previous observations of the oceanic δ^{13}C change, i.e. maximum δ^{13}C changes in the Subtropical gyre (Quay et al., 1992, 2003; Gruber et al., 1999; Sonnerup et al., 2000), is not evident in MIX. In the MIX results, the surface δ^{13}C change in the tropics was larger than in the subtropics. MIX, in this application, does not have enough near surface end-members to distinguish tropical and subtropical surface waters' changes. These waters are represented by a single end-member ('warm', Fig. 3) with only one maximum δ^{13}C perturbation value. In this application, MIX balances errors from overestimating the tropical δ^{13}C change against errors from underestimating the subtropical δ^{13}C change (Fig. 15). We have no objective basis a-priori for assigning only very small δ^{13}C changes in the 'salt' end-member, however, and such an assignment yielded substantially higher residuals overall.

Despite the longer time period covered, MIX's surface water change north of 37°N was comparable to that calculated over ∼1970–1992 from preformed δ^{13}C (Sonnerup et al., 1999). This coincidence is only possible if the subpolar North Pacific turns over rapidly enough that δ^{13}C changes occurring >20 yrs in the past aren't reflected in local surface waters. Similar to the situation described above for CFCs MIX likely underestimated the δ^{13}C change near the NPIW outcrop (north of 40°N). Although the addition of latitude dependence (eq. 4) improved the P13N CFC reconstruction, it did not measurably improve the MIX models' fit to the δ^{13}C in the WOCE P13N data or in the OGCM output. The subpolar underestimate could, in principle, also result from the anthropogenic change in an end-member not attenuating to zero anywhere within the end-members' geographic range. This is unlikely along P13N because the 'cold-fresh' end-member is present at significant levels (>10%, Fig. 3), deeper than CCl_4 measured during 1992 (Fig. 16). Within the subtropical gyre (20–35°N), the MIX anthropogenic δ^{13}C changes are approximately double the 1970–1992 δ^{13}C change (Sonnerup et al., 1999; Quay et al., 2003). In the OGCM, the simulated 1970–1992 δ^{13}C change was comparable to the reconstructions based on preformed δ^{13}C (Sonnerup et al., 1999) and station reoccupations (Quay et al., 2003), while the 1765–1992 δ^{13}C change was everywhere approximately triple the 1970–1992 change in the model.

The MIX depth-integrated ^{13}C change was largest, typically −400‰·m to −500‰·m, in the subtropics and tropics, and was smaller, approximately −200‰·m, at high latitudes. In the subpolar region, the 1765–1992 depth integrated change was comparable to that observed during 1970–1992 (Quay et al., 2003), possibly due to a tendency for MIX to underestimate the δ^{13}C change at high latitudes on this section, as discussed above. The mean industrial era depth-integrated δ^{13}C change along P13N was −377‰·m.

5. Discussion

One significant problem with the MIX approach is that it provides no readily apparent way of determining uncertainties. Goyet et al. (1999) and Coatanoan et al. (2001) took the MIX versus data residuals as an uncertainty estimate. Our experiments with CFCs and with the GCM output indicate that MIX can miss the

mark significantly and systematically even when overall residuals are small. For example, on the P13N CFC data, while MIX residuals were on the order of ±4.7% CFC saturation, in some regions MIX was off by as much as 10–20% CFC. Our error estimate for the P13N δ^{13}C change reconstruction is based on a combination of the MIX performance in reconstructing ocean CFC fields and in reconstructing the OGCM's δ^{13}C change field. These experiments indicate an average signal-to-noise up to 6–10 near the surface, but <4, i.e. a rough estimate only, in the lower thermocline (depth >500 m) along this section.

The mean industrial era (1765–1992) near-surface δ^{13}C change along the P13N section (5°S to 55°N) was −0.66‰. In the GCM, the corresponding δ^{13}C change was −0.67‰. If we tentatively adopt Bacastow et al.'s (1996) strategy of using the relationship between an OGCM's local (165°E) and global surface ocean Suess Effect (−0.81‰), we extrapolate a global surface ocean δ^{13}C change during ∼1765–1992 of -0.76 ± 0.12‰ from the 165°E MIX reconstruction. The uncertainty is based on our estimate of MIX uncertainties from the CFC and OGCM tests. We then used a one-dimensional box-diffusion model (Oeschger et al., 1975) to evaluate the constraint that this industrial era Suess effect estimate placed on ocean CO_2 uptake. The model's vertical mixing rate and gas-exchange rate were varied independently and randomly, seeking parameter combinations that reproduced the ocean's bomb-^{14}C uptake (Broecker et al., 1995) and δ^{13}C changes during 1970–1990 (Quay et al., 2003), CFC burden during 1993 (Willey et al., 2004), and the near surface δ^{13}C change during 1765–1992. The collection of model scenarios that simultaneously matched all of these tracer constraints to within $\pm 2\sigma$ indicated an ocean CO_2 uptake rate of 1.8 ± 0.2 Gt. yr^{-1} during 1970–1990, and a total anthropogenic CO_2 inventory of 112 ± 12 Gt. to Jan. 1994. These results are in excellent agreement with the 1970–1990 CO_2 uptake rate estimated based on recent δ^{13}C changes by Quay et al. (2003), and with the 1994 anthropogenic CO_2 inventory of 118 ± 17 Gt. in 1994 calculated using ΔC^* (Sabine et al.,1994). In this approach the uncertainty in the MIX lower thermocline δ^{13}C change was too large for the depth-integrated δ^{13}C change to provide an additional, useful constraint on the box-diffusion simulations. A more confident determination of the anthropogenic CO_2 burden and δ^{13}C perturbation awaits additional MIX δ^{13}C change determinations along modern δ^{13}C sections.

Our tests of MIX applied to CFCs indicated that it can provide fairly accurate estimates of anthropogenic changes in the upper ocean. In the North Pacific, density-dependent attenuation of the anthropogenic signal improved MIX's accuracy, likely because the dominant thermocline ventilation pathway is along-isopycnal there (Michel and Suess, 1975; Fine et al., 1981; Warner et al., 1996). The MIX approach's upper ocean change estimates suffer regionally when substantial trends in surface anthropogenic changes occur, as is usually the case for meridional δ^{13}C sections. Testing the MIX approach on OGCM δ^{13}C output indicated problems in deeper waters as well. Some of these problems, however, may stem from limitations of the OGCM, which may not always provide a representative test for ocean back-calculation procedures like MIX (or ΔC^*) due to this OGCM in particular's inaccurate representation of the distribution of water masses in the North Pacific Ocean. One restriction to application of MIX occurs in regions where the anthropogenic perturbation has penetrated to the bottom. In these regions MIX, as applied here, requires that the anthropogenic change attenuate to a known value at depth in at least one end-member. This would complicate MIX applications in the North Atlantic and Southern Oceans, for example. In addition, the extent to which the data set being used for MIX reconstructions represents the major regional water masses and their end-member properties is an important consideration.

Our preliminary estimate, based on only one hydrographic section, of the ocean's 1765–1992 global ^{13}C change is consistent with recent (1970s–1990s) changes in δ^{13}C (Quay et al., 2003), and with the long-term ocean CO_2 uptake estimate based on ΔC^* (Sabine et al., 2004). The MIX approach's most promising future application is in reconstructing ocean ^{13}C changes globally from the 1990s OACES/WOCE/JGOFS δ^{13}C data set (Quay et al., 2003). The resulting preindustrial δ^{13}C data set would potentially allow inversions of air-sea ^{13}C fluxes as has recently been performed for $^{12}CO_2$ only (Gurney et al., 2002), which would afford tighter constraints on the CO_2 fluxes through the terrestrial biosphere. Since the MIX approach can also be used to back-calculate ocean DIC changes (Goyet et al., 1999), simultaneous reconstructions of both δ^{13}C and $^{12}CO_2$ changes could provide estimates of the ocean's CO_2 isotopic perturbation ratio, which reflects the gas exchange equilibration efficiency of surface waters (McNeil et al., 2001). The MIX approach provides our first opportunity to calculate the ocean's anthropogenic δ^{13}C/DIC perturbation ratio with global coverage. The global ocean's δ^{13}C to DIC perturbation ratio potentially provides a constraint on the size of the exchangeable terrestrial biosphere, i.e. that part of the terrestrial biosphere (e.g. vegetation, wood, debris) that actively exchanges with the atmosphere and ocean on decadal time scales (Keir et al., 1998).

6. Acknowledgments

This manuscript was improved by thorough and thought-provoking reviews by Are Olsen and two anonymous reviewers. RES and APM were supported by NSF grants 0136907 and 0836814, respectively. The OGCM work was supported by the NOAA global carbon cycle program, GC02-391. This is JISAO contribution # 1317, PMEL # 2884.

References

Anderson, L. A. and Sarmiento, J. L. 1994. Redfield ratios of remineralization determined by nutrient data analysis. *Global Biogeochem. Cycles* **8**(1), 65–80.

Bacastow, R. B., Keeling, C. D., Lueker, T. J., Wahlen, M. and Mook, W. G. 1996. The δ^{13}C Suess effect in the world surface oceans and its implications for oceanic uptake of CO2: analysis of observations at Bermuda. *Global Biogeochem. Cycles* **10**(2), 335–346.

Battle, M., Bender, M. L., Tans, P., White, J., Ellis, J. and co-authors. 2000. Global carbon sinks and their variability inferred from atmospheric O_2 and δ^{13}C. *Science* **287**, 2467–2470.

Broecker, W. S. and Peng, T.–H. 1974. Gas exchange rates between air and sea. *Tellus* **26**, 21–35.

Broecker, W. S., Sutherland, S., Smethie, W., Peng, T.-H. and Östlund, G. 1995. Oceanic radiocarbon: Separation of the natural and bomb components. *Global Biogeochem. Cycles* **9**(2), 263–288.

Bonneau, M.-C., Bergnaud-Grazzini, C. and Berger, W. H. 1980. Stable isotope fractionation and differential dissolution in recent planktonic foraminifera from Pacific box cores. *Oceanol. Acta* **3**, 377–382.

Bullister, J. L. and Weiss, R. F. 1988. Determination of CCl_3F and CCl_2F_2 in seawater and air. *Deep-Sea Res.* **35A**, 839–853.

Coatanoan, C., Goyet, C., Gruber, N., Sabine, C. and Warner, M. 2001. Comparison of two approaches to quantify anthropogenic CO_2 in the ocean: Results from the northern Indian Ocean. *Glob. Biogeochem. Cycles* **15**(1), 11–25.

Conkright, M. E., Levitus, S. and Boyer, T. P. 1994. World Ocean Atlas 1994, Volume 1: Nutrients. NOAA Atlas NESDIS 1, U.S. Department of Commerce, NOAA, NESDIS.

Fine, R. A., Reid, J. L. and Östlund, H. G. 1981. Circulation of tritium in the Pacific Ocean. *J. Phys. Ocean.* **11**, 3–14.

Francey, R. J., Allison, C. E., Etheridge, D. M., Trudinger, C. M., Enting, I. G. and co-authors. 1999. A 1000-year high precision record of δ^{13}C in atmospheric CO_2. *Tellus* **51B**, 170–193.

Fry, B., Hopkinson, C. S., Jr., Nolin, A. and Wainright, S. C. 1998. $^{13}C/^{12}C$ composition of marine dissolved organic carbon. *Chem. Geol.* **152**, 113–118.

Gent, P. and McWilliams, J. C. 1990. Isopycnal mixing in ocean circulation models. *J. Phys. Ocean.* **20**, 150–155.

Gnanadesikan, A., Slater, R. D., Gruber, N. and Sarmiento, J. L. 2002. Oceanic vertical exchange and new production: a comparison between models and observations. *Deep-Sea Research II* **49**, 363–401.

Goericke, R. and Fry, B. 1994. Variations of marine plankton δ^{13}C with latitude, temperature, and dissolved CO_2 in the world ocean. *Global Biogeochem. Cycles* **8**(1), 85–90.

Goyet, C. and Davis, D. 1997. Estimation of total CO_2 concentration throughout the water column. *Deep-Sea Res.* **44**(5), 859–877.

Goyet, C., Coatanoan, C., Eischeid, G., Amaoka, T., Okuda, K. and co-authors. 1999. Spatial variation of total CO_2 and total alkalinity in the northern Indian Ocean: A novel approach for the quantification of anthropogenic CO_2 in seawater. *J. Mar. Res.* **57**, 135–163.

Gruber, N. and Keeling, C. D. 2001. An improved estimate of the isotopic air-sea disequilibrium of CO_2: Implications for the oceanic uptake of anthropogenic CO_2. *Geophys. Res. Lett.* **28**(3), 555–558.

Gruber, N., Keeling, C. D., Bacastow, R. B., Guenther, P. R., Lueker, T. J. and co-authors. 1999. Spatiotemporal patterns of carbon-13 in the global surface oceans and the oceanic Suess effect. *Global Biogeochem. Cycles* **13**(2), 307–335.

Gruber, N., Sarmiento, J. L. and Stocker, T. F. 1996. An improved method for detecting anthropogenic CO_2 in the oceans. *Global Biogeochem. Cycles* **10**(4), 809–837.

Gurney, K. R., Law, R. M., Denning, A. S., Rayner, P. J., Baker, D. and co-authors. 2002. Towards robust regional estimates of CO_2 sources and sinks using atmospheric transport models. *Nature* **415**, 626–630.

Heimann, M. and Maier-Reimer, E. 1996. On the relations between the oceanic uptake of CO2 and its carbon isotopes. *Glob. Biogeochem. Cycles* **10**(1), 89–110.

Hellerman, S. and Rosenstein, M. 1983. Normal monthly wind stress over the world ocean with error estimates. *J. Phys. Ocean.* **13**, 1093–1104.

Huang, R.-X. and Qiu, B. 1998. The structure of the wind-driven circulation in the subtropical South Pacific Ocean. *J. Phys. Ocean.* **28**, 1173–1186.

Huhn, O., Roether, W., Beining, P. and Rose, H. 2001. Validity limits of carbon tetrachloride as an ocean tracer. *Deep-Sea Res. I* **48**, 2025–2049.

Johnson, G. C. and McPhaden, M. J. 1999. Interior pycnocline flow from the subtropical to the equatorial Pacific Ocean. *J. Phys. Ocean.* **29**, 3073–3089.

Karstensen, J. and Tomczak, M. 1998. Age determination of mixed water masses using CFC and oxygen data. *J. Geophys. Res.*, **103**(C9), 18599–18610.

Keir, R. S., Rehder, G., Suess, E. and Erlenkeuser, H. 1998. The δ^{13}C anomaly in the Northeastern Atlantic. *Global Biogeochem. Cycles* **12**(3), 467–477.

Kroopnick, P. M. 1985. The distribution of δ^{13}C of ΣCO_2 in the world oceans. *Deep-Sea Res.* **32**(1), 57–84.

Matear, R. J. and McNeil, B. I. 2003. Decadal accumulation of anthropogenic CO_2 in the Southern Ocean: A comparison of CFC-age derived estimates to multiple-linear regression estimates. *Global Biogeochem. Cycles* **17**(4), 1113, doi:10.1029(2003GB002089.

Matsumoto, K., Sarmiento, J. L., Key, R. M., Aumont, O., Bullister, J. L. and co-authors. 2004. Evaluation of ocean carbon cycle models with data-based metrics. *Geophys. Res. Lett.* **31**, L07303, doi:10.1029(2003GL018970.

McNeil, B. I., Matear, R. J. and Tilbrook, B. 2001. Does carbon 13 track anthropogenic CO_2 in the Southern Ocean?. *Global Biogeochem. Cycles* **15**(3), 597–613.

McNeil, B. I., Matear, R. J., Key, R. M., Bullister, J. L. and Sarmiento, J. L. 2003. Anthropogenic CO_2 uptake by the ocean based on the global chlorofluorocarbon data set. *Science* **229**, 235–239.

Michel, R. L. and Suess, H. E. 1975. Bomb tritium in the Pacific Ocean. *J. Geophys. Res.* **80**, 4139–4152.

Monterey, G. I. and Levitus, S. 1997. *Climatological cycle of mixed layer depth in the world ocean*. U. S. Govt. Printing Office, NOAA NESDIS, pp. 5.

Oeschger, H., Siegenthaler, U., Schotterer, U. and Gugelmann, A. 1975. A box-diffusion model to study carbon dioxide in nature. *Tellus* **28**, 168–192.

Orr, J. C. 2002. Global ocean storage of anthropogenic carbon (GOSAC), Final report to the EC environment and climate Programme. ENV4-CT97–0495.

Pacanowski, R. C. and Griffies, S. M. 1999. The MOM 3 manual, alpha version. NOAA(Geophysical Fluid Dynamics Laboratory, 580 pp.

Pickard, G. L. and Emery, W. J. 1990. *Descriptive Physical Oceanography*. Pergamon press, New York, pp 320.

Quay, P. D., Tilbrook, B. and Wong, C. S. 1992. Oceanic uptake of fossil-fuel CO_2: Carbon-13 evidence. *Science* **256**, 74–79.

Quay, P. D., Sonnerup, R. E., Westby, T., Stutsman, J. and McNichol, A. P. 2003. Anthropogenic changes of the $^{13}C/^{12}C$ of dissolved inorganic carbon in the ocean as a tracer of CO_2 uptake. *Global Biogeochem. Cycles* **17**(1), 1004, doi:10.1029(2001GB001817.

Redfield, A. C., Ketchum, B. H. and Richards, F. A. 1963. The influence of organisms on the composition of sea-water. In: *The Sea*, vol. 2. (ed. M. N. Hill), Interscience, New York pp. 26–77.

Sabine, C. L., Feely, R. A., Gruber, N., Key, R. M., Lee, K. and co-authors. 2004. The oceanic sink for anthropogenic CO_2. *Science* **305**, 367–371.

Sonnerup, R. E., Quay, P. D., McNichol, A. P., Bullister, J. L., Westby, T. A. and co-authors. 1999. Reconstructing the oceanic 13C Suess effect. *Global Biogeochem. Cycles* **13**(4), 857–872.

Sonnerup, R. E., Quay, P. D. and McNichol, A. P. 2000. The Indian Ocean ^{13}C Suess effect. *Global Biogeochem. Cycles* **14**(3), 903–916.

Stuiver, M., Quay, P. D. and Östlund, H. G. 1983. Abyssal water Carbon-14 distribution and the age of the world oceans. *Science* **219**(4586), 849–851.

Takahashi, T., Sutherland, S. C., Sweeney, C., Poisson, A., Metzl, N. and co-authors. 2002. *Deep-Sea Res.* **49**, 1601–1622.

Takahashi, Y., Matsumoto, E. and Watanabe, Y. W. 2000. The distribution of $\delta^{13}C$ in total dissolved inorganic carbon in the central North Pacific Ocean along 175°E and implications for anthropogenic CO_2 penetration. *Marine Chemistry* **69**, 237–251.

Tomczak, M. and Large, D. G. B. 1989. Optimum multiparameter analysis of mixing in the thermocline of the eastern Indian Ocean. *J. Geophys. Res.* **94**(C11), 16141–16149.

Wallace, D. W. R. 1995. Monitoring global ocean carbon inventories. Ocean Observing System Development Panel, Texas A&M University, College Station, TX, 54 pp.

Warner, M. J., Bullister, J. L., Wisegarver, D. P., Gammon, R. H. and Weiss, R. F. 1996. Basinwide distributions of chlorofluorocarbons CFC-11 and CFC-12 in the North Pacific: 1985–1989. *J. Geophys. Res.* **101**, 20525–20542.

Warner, M. J. and Weiss, R. F. 1985. Solubilities of chlorofluorocarbons 11 and 12 in water and seawater. *Deep-Sea Res.* **32**, 1485–1497.

Watanabe, Y. W., Ono, T. and Shimamoto, A. 2000. Increase in the uptake rate of oceanic anthropogenic carbon in the North Pacific determined by CFC ages. *Mar. Chem.* **72**, 297–315.

Waugh, D. W., Hall, T. M. and Haine, T. W. N. 2003. Relationships among tracer ages. *J. Geophys. Res.* **108**(C5), 3138, doi: 10.1029(2002(JC001325.

Willey, D. A., Fine, R. A., Sonnerup, R. E., Bullister, J. L., Smethie, W. M., Jr. and Warner, M. J. 2004. Global oceanic chlorofluorocarbon inventory. *Geophysical Research LettersGeophys. Res. Lett.* **31**, L01303, doi:10.1029(2003GL018816.

Zhang, J., Quay, P. D. and Wilbur, D. O. 1995. Carbon isotope fractionation during gas-water exchange and dissolution of CO_2. *Geochemica et Cosmochimica Acta* **59**(1), 107–114.